JOURNAL OF GEOPHYSICAL RESEARCH, VOL. 111, D16307, doi:10.1029/2005JD006696, 2006

Inverse modeling of the global methyl chloride sources

Yasuko Yoshida,[1] Yuhang Wang,[1] Changsub Shim,[1] Derek Cunnold,[1] Donald R. Blake,[2] and Geoffrey S. Dutton[3]

Received 22 September 2005; revised 24 February 2006; accepted 26 April 2006; published 23 August 2006.

[1] Inverse modeling using the Bayesian least squares method is applied to better constrain the sources and sinks of atmospheric methyl chloride (CH_3Cl) using observations from seven surface stations and eight aircraft field experiments. We use a three-dimensional global chemical transport model, the GEOS-Chem, as the forward model. Up to 39 parameters describing the continental/hemispheric and seasonal dependence of the major sources of CH_3Cl are used in the inversion. We find that the available surface and aircraft observations cannot constrain all the parameters, resulting in relatively large uncertainties in the inversion results. By examining the degrees of freedom in the inversion Jacobian matrix, we choose a reduced set of parameters that can be constrained by the observations while providing valuable information on the sources and sinks. In particular, we resolve the seasonal dependence of the biogenic and biomass-burning sources for each hemisphere. The in situ aircraft measurements are found to provide better constraints on the emission sources than surface measurements. The a posteriori emissions result in better agreement with the observations, particularly at southern high latitudes. The a posteriori biogenic and biomass-burning sources decrease by 13 and 11% to 2500 and 545 Gg yr^{-1}, respectively, while the a posteriori net ocean source increases by about a factor of 2 to 761 Gg yr^{-1}. The decrease in biomass-burning emissions is largely due to the reduction in the emissions in seasons other than spring in the Northern Hemisphere. The inversion results indicate that the biogenic source has a clear winter minimum in both hemispheres, likely reflecting the decrease of biogenic activity during that season.

Citation: Yoshida, Y., Y. Wang, C. Shim, D. Cunnold, D. R. Blake, and G. S. Dutton (2006), Inverse modeling of the global methyl chloride sources, *J. Geophys. Res.*, *111*, D16307, doi:10.1029/2005JD006696.

1. Introduction

[2] Methyl chloride (CH_3Cl) is one of the most abundant chlorine-containing gases in the atmosphere and a major contributor to the stratospheric chlorine loading. The global average mixing ratio of CH_3Cl in the troposphere is measured at about 550 ± 30 parts per trillion per volume (pptv); a major concern about this species is the imbalance of its budget, i.e., known sinks are much larger than known sources [e.g., *Montzka et al.*, 2003].

[3] According to the emission data provided in the Reactive Chlorine Emissions Inventory (RCEI) conducted under the International Global Atmospheric Chemistry (IGAC) Global Emissions Inventory Activity (GEIA) project, the estimated emissions from known sources such as biomass-burning, oceans, incineration/industrial sources are 910 (650–1120), 650 (40–950), and 162 (30–294) Gg (giga gram = 10^9 gram) yr^{-1}, respectively [*Keene et al.*, 1999; *Khalil et al.*, 1999; *Lobert et al.*, 1999; *McCulloch et al.*, 1999] (the numbers are best estimates with full ranges in the parenthesis). Emission from certain wood-rotting fungi is estimated as 156 (35–385) Gg yr^{-1}, though no global distribution is currently available [*Watling and Harper*, 1998; *Khalil et al.*, 1999; *Lee-Taylor et al.*, 2001]. In addition, *Rhew et al.* [2000] estimated annual global release of 170 (65–440) Gg of CH_3Cl from salt marshes, and *Varner et al.* [1999] calculated a global flux of 48 Gg yr^{-1} from wetlands.

[4] The major removal process of CH_3Cl in the atmosphere is due to oxidation by OH radicals, which accounts for a 3.5 (2.8–4.6) Tg (teragram = 10^{12} gram) loss per year [*Koppmann et al.*, 1993]. It is estimated that about 285 Gg of tropospheric CH_3Cl is transported to the stratosphere and lost there by photo dissociation and OH oxidation. Although the ocean is a net source globally, it is a significant net local sink in high-latitude regions. The RCEI estimate for the oceanic sink over the net uptake regions is 150 Gg yr^{-1} [*Moore et al.*, 1996; *Khalil et al.*, 1999; *Keene et al.*, 1999]. Soil is recognized as an additional sink, and *Keene et al.* [1999] estimated that it could be as much as 256 Gg yr^{-1}, but the uncertainty is quite high [*Lee-Taylor et*

[1]School of Earth and Atmospheric Sciences, Georgia Institute of Technology, Atlanta, Georgia, USA.
[2]Department of Chemistry, University of California, Irvine, California, USA.
[3]NOAA Climate Monitoring and Diagnostics Laboratory and Cooperative Institute for Research in Environmental Sciences, Boulder, Colorado, USA.

0148-0227/06/2005JD006696$09.00

al., 2001; *Rhew et al.*, 2001]. The CH_3Cl budget based on the current "best guess" estimates given above leaves a substantial source deficit of $\sim$1.8 Tg yr^{-1}.

[5] There is experimental and modeling evidence that the missing source is biogenic in origin. Enhancements of CH_3Cl that are correlated with a short-lived biogenic tracer (α-pinene) were measured by *Yokouchi et al.* [2000]. *Yokouchi et al.* [2002] found strong emissions of CH_3Cl from tropical plants, although the biological processes responsible for the emissions from terrestrial vegetation are unknown [*Keene et al.*, 1999; *Yokouchi et al.*, 2000, 2002].

[6] *Khalil and Rasmussen* [1999] suggested that 85% of the emission of CH_3Cl comes from tropical and subtropical regions on the basis of their inverse modeling results with simplified box models for tropospheric transport and OH oxidation. *Hamilton et al.* [2003] estimated a global annual CH_3Cl production of 75–2500 Gg between 30°N and 30°S on the basis of their CH_3Cl flux observations from senescent and dead leaves. In a global three-dimensional (3-D) model simulation of CH_3Cl, *Lee-Taylor et al.* [2001] found that a biogenic source of 2330–2430 Gg yr^{-1} is necessary for the model to reproduce surface observations of CH_3Cl.

[7] We also conducted and evaluated global 3-D model simulations of CH_3Cl with aircraft in situ measurements taken in field experiments from 1991 to 2001 as well as surface site measurements [*Yoshida et al.*, 2004]. As in the work by *Lee-Taylor et al.* [2001], we included a large biogenic source of 2900 Gg yr^{-1} in order to explain the observed CH_3Cl distributions. The source is limited to the region between 30°S and 30°N in order to reproduce the observed seasonal and latitudinal variations in the model. We assume that the source is aseasonal because no a priori information is currently available to specify temporal variability of the source in the model. One of the major problems in the model simulations is the overestimate of the seasonal variation of CH_3Cl at southern middle and high latitudes.

[8] We explore in this work a different approach [from *Yoshida et al.*, 2004] to analyze the surface and aircraft observations. The question we pose is to what extent the seasonal and geographical dependence of the biogenic and other sources can be constrained by the available observations. We apply a Bayesian least squares method to derive the CH_3Cl sources on the basis of the measurements from seven surface sites and eight aircraft field experiments. The "bottom-up" inventories by *Yoshida et al.* [2004] are used as a priori. By inspecting the Jacobian matrix and inversion results, we examine the number of emission parameters that can be constrained and compare the constraints by the surface measurements to those by aircraft measurements.

2. Methods

2.1. Observations

[9] The observations of CH_3Cl from seven surface stations and eight aircraft missions are used in this study. Table 1 summarizes these measurements. The locations of the surface measurement sites and aircraft observation regions are shown in Figure 1. There are two measurement data sets for Alaska, Hawaii, Samoa, Tasmania and Antarctica. Both are used in the inversion. For aircraft observa-

Table 1. Atmospheric Measurements of CH_3Cl[a]

	Region	Time Period	Reference
	Surface Sites		
Khalil and Rasmussen [1999]	Alaska (71.2°N, 156.5°W), Oregon (45.5°N, 124°W), Hawaii (19.3°N, 154.5°W), Samoa (14.1°S, 170.6°W), Tasmania (42°S, 145°E), Antarctica (90°S)	1981–1997	*Khalil and Rasmussen* [1999]
NOAA CMDL	Alaska (71.3°N, 156.6°W)	Jan. 1998 to March 2002	G. Dutton (personal communication, 2004)
NOAA CMDL	Hawaii (19.5°N, 155.6°W)	Dec. 1999 to Feb. 2002	G. Dutton (personal communication, 2004)
NOAA CMDL	Samoa (14.2°S, 170.6°W)	Dec. 1998 to Feb. 2003	G. Dutton (personal communication, 2004)
NOAA CMDL	Antarctica (90.0°S, 102.0°E)	Jan. 2001 to Nov. 2003	G. Dutton (personal communication, 2004)
AGAGE	Ireland (53.2°N, 9.5°W), Tasmania (40.4°S, 144.4°E)	1998–2001	*Simmonds et al.* [2004]
	Aircraft Missions		
PEM-Tropics A	tropical Pacific	Aug.–Oct. 1996	*Blake et al.* [1999a]
PEM-Tropics B	tropical Pacific	March–April 1999	*Blake et al.* [2001]
ACE 1	Pacific/Southern Ocean	Nov.–Dec. 1995	*Blake et al.* [1999b]
TRACE-A	tropical Atlantic	Sept.–Oct. 1992	*Blake et al.* [1996]
PEM-West A	western Pacific	Sept.–Oct. 1991	*Blake et al.* [1997]
PEM-West B	western Pacific	Feb.–March 1994	*Blake et al.* [1997]
TRACE-P	western Pacific	Feb.–April 2001	*Blake et al.* [2003b]
TOPSE	North America	Feb.–May 2000	*Blake et al.* [2003a]

[a]NOAA CMDL, National Oceanic and Atmospheric Administration Climate Monitoring and Diagnostics Laboratory; AGAGE, Advanced Global Atmospheric Gases Experiment; PEM, Pacific Exploratory Mission; ACE 1, First Aerosol Characterization Experiment; TRACE-A, Transport and Chemical Evolution over the Atlantic; TRACE-P, Transport and Chemical Evolution over the Pacific; TOPSE, Tropospheric Ozone Production about the Spring Equinox.

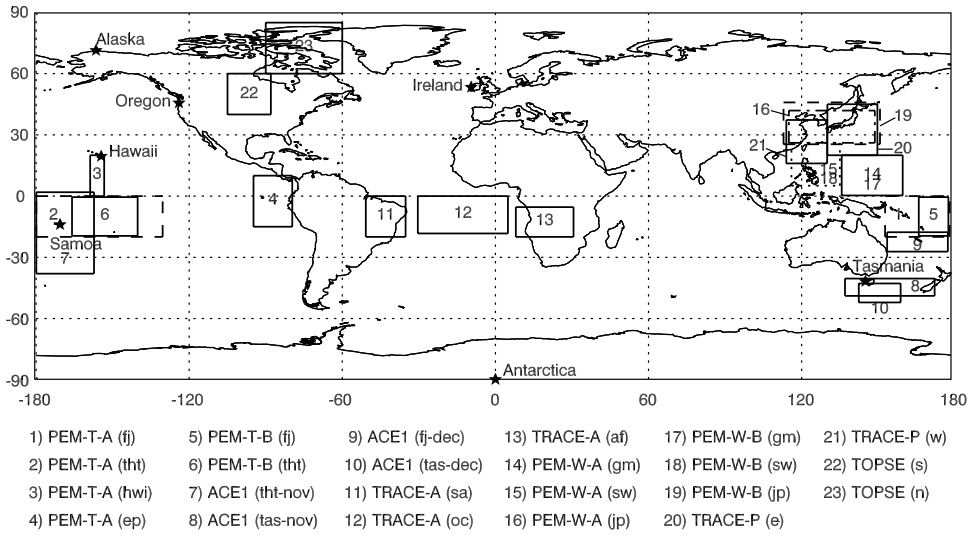

Figure 1. Surface measurement sites (indicated by symbols) and aircraft observation regions. The measurements are listed in Table 1. Here, fj, Fiji; tht, Tahiti; hwi, Hawaii; ep, eastern Pacific; tas, Tasmania; sa, South America; oc, South Atlantic; af, southern Africa; gm, Guam; sw, southwest; jp, Japan.

tions, the experiment regions are divided into 23 smaller regions [*Yoshida et al.*, 2004]. We calculate monthly mean concentrations for each data set for model evaluation and inversion calculation. In order to compare the constraints on the CH_3Cl sources by surface measurements with those by aircraft measurements, inverse modeling is conducted using three data sets: (1) data from station observations only, (2) data from aircraft experiments only, and (3) data from both station and aircraft experiments.

2.2. Forward Model

2.2.1. Model Description

[10] The model used in this study is the GEOS-Chem (version 5.02) global 3-D chemical transport model (CTM) of tropospheric chemistry driven by assimilated meteorological fields from the Goddard Earth Observing System (GEOS) of the NASA Global Modeling and Assimilation Office (GMAO) (http://www-as.harvard.edu/chemistry/trop/geos/) [*Bey et al.*, 2001]. We use a horizontal resolution of 4° latitude × 5° longitude and 26 vertical levels. We simulate the CH_3Cl distributions using meteorological fields for August 1996 to September 1997 (GEOS-STRAT). In our previous work [*Yoshida et al.*, 2004], we used the assimilated meteorology for different years and found that the resulting difference in CH_3Cl distributions is relatively small. This uncertainty is now accounted for as part of the model transport error (section 2.3.3). CH_3Cl increase (decrease) by a source (sink) is "tagged" by a different tracer. In this manner, the contribution from a source or sink to the spatial and temporal CH_3Cl distributions can be evaluated in the model. The sink by OH oxidation is not treated as a separate tracer; the uncertainties of the OH field and reaction rate constant are taken into account as part of the model error (section 2.3.3).

2.2.2. Sources and Sinks of CH_3Cl

[11] Our a priori sources of CH_3Cl are taken from the best estimates by *Yoshida et al.* [2004]. Table 2 summarizes the annual emissions and the sinks. We briefly describe here the sources and sinks. More detailed discussion can be found in the previous work [*Yoshida et al.*, 2004, and references therein].

[12] We distribute the biogenic source of 2900 Gg yr^{-1} to all vegetated areas between 30°N and 30°S with a flat aseasonal emission rate [*Yoshida et al.*, 2004]. We compute biomass-burning CH_3Cl emissions using a CH_3Cl/CO molar emission ratio [*Lobert et al.*, 1999] with the 7-year mean of the GEOS-Chem biomass and biofuel burning CO emissions between 1991 and 2001 [*Duncan et al.*, 2003; *Heald et al.*, 2003]. The resulting annual total biomass-burning CH_3Cl emission is about 610 Gg yr^{-1}, which is at the lower limit calculated by *Lobert et al.* [1999].

[13] The oceanic CH_3Cl emissions and sinks are calculated using the National Oceanic and Atmospheric Administration Climate Monitoring and Diagnostics Laboratory (NOAA-CMDL) empirical relationship between saturation and sea surface temperature (SST) and CH_3Cl saturation anomaly [*Khalil et al.*, 1999] with monthly climatological wind speed distributions. Oceanic sink is scaled so that the net oceanic flux is to be ~350 Gg yr^{-1} [*Yoshida et al.*, 2004].

[14] The tropospheric OH field is taken from the GEOS-Chem full chemistry simulation by *Martin et al.* [2003] and the stratospheric OH field is taken from a 2-D stratosphere/mesosphere model [*Schneider et al.*, 2000]. Chemical loss of CH_3Cl via OH oxidation is calculated using reaction rate constant reported by *Sander et al.* [2003]. The a priori total CH_3Cl loss by reaction with OH is about 3990 Gg yr^{-1}. The estimated soil sink of 256 Gg yr^{-1} [*Keene et al.*, 1999; *Khalil and Rasmussen*, 1999] is distributed on the basis of the work by *Shorter et al.* [1995] for growing seasons.

2.3. Inverse Model

2.3.1. Inversion Methods

[15] A Bayesian least squares method is applied in order to optimize the a priori source strengths and seasonality using the observed atmospheric CH_3Cl concentrations. The observation vector **y** of CH_3Cl measurements can be

Table 2. CH_3Cl Sources and Sinks and Their Uncertainties

				39 Parameters			16 Parameters			11 Parameters		
	Hemisphere and Season	A Priori Flux, Gg yr^{-1}	Reference	A Posteriori Flux, Gg yr^{-1}	A Priori Uncertainty, %	A Posteriori Uncertainty, %	A Posteriori Flux Gg yr^{-1}	A Priori Uncertainty, %	A Posteriori Uncertainty, %	A Posteriori Flux, Gg yr^{-1}	A Priori Uncertainty, %	A Posteriori Uncertainty, %
Biogenic	NH spring	343[a]		342	100	91	359	100	61	406	100	38
Biogenic	NH summer	343[a]		299	100	90	279	100	56	299	100	55
Biogenic	NH fall	340[a]		355	100	73	407	100	45	401	100	38
Biogenic	NH winter	336[a]		192	100	84	138	100	40	162	100	40
NH total		1362[a]		1188			1183			1268		
Biogenic	SH fall	388[a]		359	100	89	381	100	55	399	100	32
Biogenic	SH winter	388[a]		254	100	85	187	100	47	127	100	42
Biogenic	SH spring	383[a]		420	100	60	424	100	35	395	100	32
Biogenic	SH summer	379[a]		354	100	84	359	100	40	320	100	39
SH total		1538[a]		1387			1351			1241		
Global total		2900[a]	2430[b]	2575			2534			2509		
Biomass burning	NH spring	141[a,c]		143	70	61	138	70	63	119	70	55
Biomass burning	NH other seasons	244[a,c]		197	70	67	160	70	64	162	70	61
Biomass burning	SH spring	98[a,c]		115	70	65	115	70	66	116	70	62
Biomass burning	SH other seasons	127[a,c]		118	70	69	115	70	68	148	70	62
Total		610[a,c]	910[c]	573			528			545		
Ocean		507[a,d]	805[d]	760	70[d]	49	824	70[d]	52	806	70	51
Incineration/industry		162[e]	162[e]	129	80[e]	66	98	100	63	49	100	56
Salt marshes		170[f]	170[f]	96	100	91	103	100	63	51	100	56
Wetlands		48[g]	48[g]	41	100	98	29	100	63	14	100	56
Total source		4397	4525	4173			4116			3974		
Ocean sink		149[a,d]	150[d]	94	70[d]	50	88	70[d]	51	45	100	56
Soil sink		256[h]	256[h]	234	100	85	179	100	83	77	100	56
OH sink		3992[a]	3500[i]	3845			3848			3852		
Total sink		4397	3906	4173			4116			3974		

[a] *Yoshida et al.* [2004].
[b] *Lee-Taylor et al.* [2001].
[c] *Lobert et al.* [1999].
[d] *Khalil et al.* [1999].
[e] *McCulloch et al.* [1999].
[f] *Rhew et al.* [2000].
[g] *Varner et al.* [1999].
[h] *Khalil and Rasmussen* [1999] and *Keene et al.* [1999].
[i] *Koppmann et al.* [1993].

Table 3. Model Parameters in the State Vector

	Region	Season (Months)	39 Parameters	16 Parameters[a]	11 Parameters[a]
Biogenic	North America	spring (3–5)	1	1	1
Biogenic	North America	summer (6–8)	2	2	2
Biogenic	North America	fall (9–11)	3	3	1
Biogenic	North America	winter (12,1,2)	4	4	3
Biogenic	South America	fall (3–5)	5	5	4
Biogenic	South America	winter (6–8)	6	6	5
Biogenic	South America	spring (9–11)	7	7	4
Biogenic	South America	summer (12,1,2)	8	8	6
Biogenic	North Africa	spring (3–5)	9	1	1
Biogenic	North Africa	summer (6–8)	10	2	2
Biogenic	North Africa	fall (9–11)	11	3	1
Biogenic	North Africa	winter (12,1,2)	12	4	3
Biogenic	South Africa	fall (3–5)	13	5	4
Biogenic	South Africa	winter (6–8)	14	6	5
Biogenic	South Africa	spring (9–11)	15	7	4
Biogenic	South Africa	summer (12,1,2)	16	8	6
Biogenic	Asia	spring (3–5)	17	1	1
Biogenic	Asia	summer (6–8)	18	2	2
Biogenic	Asia	fall (9–11)	19	3	1
Biogenic	Asia	winter (12,1,2)	20	4	3
Biogenic	Oceania	fall (3–5)	21	5	4
Biogenic	Oceania	winter (6–8)	22	6	5
Biogenic	Oceania	spring (9–11)	23	7	4
Biogenic	Oceania	summer (12,1,2)	24	8	6
Biomass burning	NH	spring (3–5)	25	9	7
Biomass burning	NH	summer (6–8)	26	10	8
Biomass burning	NH	fall (9–11)	27	10	8
Biomass burning	NH	winter (12,1,2)	28	10	8
Biomass burning	SH	fall (3–5)	29	11	9
Biomass burning	SH	winter (6–8)	30	11	9
Biomass burning	SH	spring (9–11)	31	12	9
Biomass burning	SH	summer (12,1,2)	32	11	9
Ocean emission			33	13	10
Incineration/industrial			34	14	11
Salt marshes			35	14	11
Wetlands			36	14	11
Ocean sink			37	15	11
NH soil sink			38	16	11
SH soil sink			39	16	11

[a]In the 16- and 11-parameter cases, parameters with the same number indicate that they are lumped as a single parameter.

explained by the state vector $\mathbf{x}$ of source/sink model parameters by the following equation:

$$\mathbf{y} = \mathbf{K}\mathbf{x} + \varepsilon_{\Sigma}, \tag{1}$$

where $\mathbf{K}$ is the Jacobian matrix, which relates the source parameters to the concentrations, and ε_{Σ} is the total observational error, which includes measurement error, representation error, and forward model error. The optimal solution for the state vector ($\hat{\mathbf{x}}$) and the a posteriori error covariance matrix ($\hat{\mathbf{S}}$) are

$$\hat{\mathbf{x}} = \mathbf{x}_a + \mathbf{S}_a\mathbf{K}^T\left(\mathbf{K}\mathbf{S}_a\mathbf{K}^T + \mathbf{S}_{\Sigma}\right)^{-1}\left(\mathbf{y} - \mathbf{K}\mathbf{x}_a\right) \tag{2}$$

$$\hat{\mathbf{S}} = \left(\mathbf{K}^T\mathbf{S}_{\Sigma}^{-1}\mathbf{K} + \mathbf{S}_a^{-1}\right)^{-1}, \tag{3}$$

where $\mathbf{x}_a$ is the a priori parameter state vector, $\mathbf{S}_a$ is the a priori parameter error covariance matrix, and $\mathbf{S}_{\Sigma}$ is the observation error covariance matrix [*Rodgers*, 2000]. Detailed explanation of $\mathbf{S}_{\Sigma}$ is in section 2.3.3.

[16] We apply equations (2) and (3) to the data set that contain both station and aircraft observations described in section 2.1. In the sensitivity analysis, we also apply station and aircraft data separately in the inversion.

2.3.2. Selection of the State Vector

[17] Ideally, we wish to constrain the geographical and seasonal distributions of all CH_3Cl sources. However, the available measurements usually provide a limited number of degrees of freedom. The independence of the parameters in our state vector is assessed by inspecting the singular values of the error-normalized Jacobian matrix [*Rodgers*, 2000]:

$$\tilde{\mathbf{K}} = \mathbf{S}_{\Sigma}^{-1/2}\mathbf{K}\mathbf{S}_a^{1/2}. \tag{4}$$

[18] The largest a priori sources are biogenic and biomass burning. The constraints on the biogenic sources are most interesting because of a lack of a priori knowledge. We therefore choose 24 emission parameters for this source representing 4 seasons and 6 continents (north and south Americas, north and south Africa, Asia and Oceania). We specify 8 emission parameters for the biomass-burning source in 4 seasons and 2 hemispheres. Adding 7 emission parameters for other source, there are a total of 39 emission parameters (Table 3) in our initial inversion analysis. The

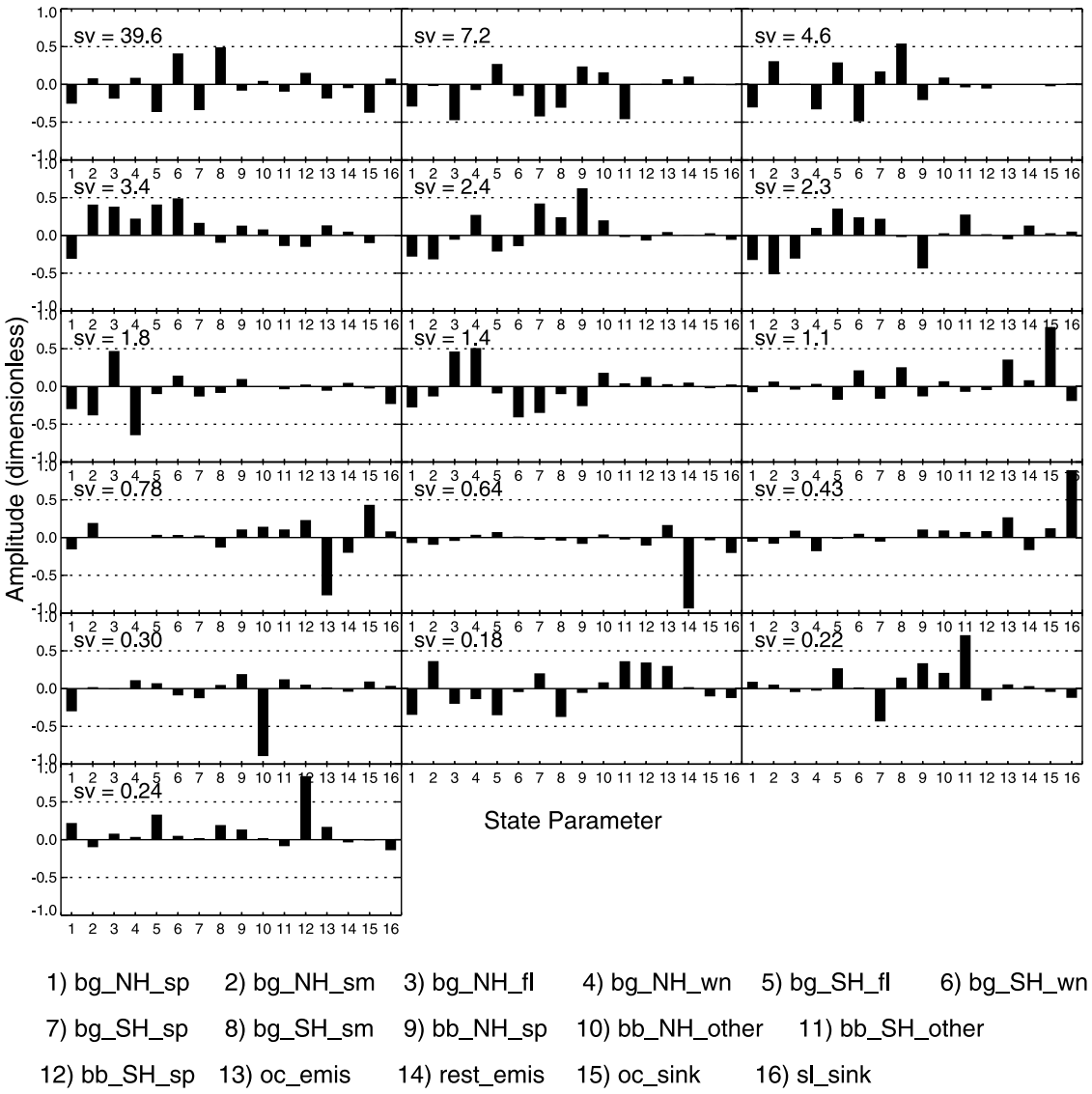

Figure 2. Singular vectors of the prewhitened Jacobian matrix $\tilde{\mathbf{K}}$ for the 16-parameter case. Here, "bg," "bb," "oc," and "sl" denote biogenic, biomass burning, ocean, and soil, respectively. Spring, summer, fall, and winter are denoted by "sp," "sm," "fl," and "wn," respectively.

degree of freedom defined by singular values >1 of the Jacobian matrix is 10; clearly indicating that current available observations do not provide enough constraints on all estimates of emission parameters.

[19] Following the approach by *Heald et al.* [2004], we then reduce the number of emissions parameters largely by aggregating the continental biogenic emissions to hemispheric ones. The benefit of the approach is that we obtain physically meaningful results compared to the vector mapping method by *Rodgers* [2000]. However, the approach also makes an implicit assumption that the lumped sources have predetermined distributions. The resulting 16 parameters are listed in Table 3. The analysis serves two purposes. First, we will investigate the effect of reducing the number of parameters on the inversion results. Second, we examine the singular vectors of $\tilde{\mathbf{K}}$ (Figure 2) in order to combine highly correlated emission parameters together. The final 11 emission parameters are listed in Table 3. The degree of freedom in the inversion is 10. In order to check the quality of our inversion results, also examine the averaging kernel matrix [*Rodgers*, 2000]:

$$\mathrm{A} = \mathrm{GK}, \tag{5}$$

where $\mathrm{G} = \mathbf{S}_a\mathbf{K}^T(\mathbf{K}\mathbf{S}_a\mathbf{K}^T + \mathbf{S}_\Sigma)^{-1}$.

2.3.3. Error Estimation

[20] A priori parameter errors are listed in Table 2. We assume that the emission errors are uncorrelated. *Lobert et al.* [1999] suggested an uncertainty of about 30% for biomass-burning CH_3Cl emissions. It is relatively low because only the uncertainty in the CH_3Cl/CO molar emission ratio is accounted for. We include the 50% uncertainty for the biomass-burning emissions of CO [*Palmer et al.*, 2003] and calculate an uncertainty of 70% for the biomass-burning emissions. We assign an uncertainty of 70% to oceanic flux [*Khalil et al.*, 1999]. The uncertainty

for incineration/industrial source is about 80% [*McCulloch et al.*, 1999]. We assign 100% of uncertainty to the salt marsh and wetland sources. For the aggregated parameter of the minor sources of incineration/industrial, salt marshes, wetlands and oceanic sink, we use an uncertainty of 100% in the 16- and 11-parameter cases. Direct estimates for the a priori biogenic emissions are unavailable. However, the total source of CH_3Cl is constrained relatively well by its main sink, the OH oxidation. Further considering the uncertainties of other better known sources, we assign an uncertainty of 100% to the biogenic source.

[21] The observational error covariance $\mathbf{S}_\Sigma$ in equation (2) is the sum of the covariance matrices of individual error types including the measurement errors, the representation error, and the forward model error. These errors are assumed to be uncorrelated. The measurement error is relatively small ($\sim$1%). The representation error is calculated as the standard deviation of the observations for each data grid. The forward model error includes the transport error estimated using the relative residual error (RRE) method by *Palmer et al.* [2003], the 7-year interannual variability of modeled CH_3Cl calculated by *Yoshida et al.* [2004], and the errors associated with the OH field (14%) [*Prinn et al.*, 2001] and OH + CH_3Cl kinetics (15%) [*Sander et al.*, 2003]. The total observational error is calculated as the product of square root mean of relative error of each error types and the observation value of CH_3Cl; and the mean observational error is about 21%.

3. Results

[22] Through inversion, we evaluate the constraints on the estimates of distributions and seasonal variations of CH_3Cl sources and sinks provided by surface and aircraft observations. We first investigate the effects of the state vector size on the inversion results. The state vectors in the three inversion cases (section 2.3.2) have 39, 16, and 11 parameters, respectively. The averaging kernels (rows of A in equation (5)) show clear peaks at the appropriate level for 16- and 11-parameter cases, indicating those parameters are independent. Parameters lacking with a significant peak such as biomass burning have large a posteriori error in consequence.

3.1. Sensitivity to State Vector Size

3.1.1. Monthly Flux

[23] The a priori and a posteriori monthly CH_3Cl fluxes are shown in Figure 3. The annual total of each source/sink is listed in Table 2. The a posteriori fluxes are generally consistent despite the large difference in the state vector size. The more apparent effect of the state vector size is on the uncertainties of the a posteriori emissions. It is particularly large for the biogenic source. The a posteriori uncertainties decrease from 60–90% for 39 parameters to 35–60% for 16 parameters, and further to 32–40% for 11 parameters. The uncertainty decrease is expected as the number of parameters approaches to the degree of freedom in inversion. The a posteriori uncertainties for the other sources also decrease with the parameter number but not to the extent of the biogenic sources.

[24] The a posteriori biogenic sources show a clear winter minimum. The Northern Hemisphere (NH) decrease is 50–60% from spring/fall. The seasonal decrease of 40–70% from spring/fall is more variable in the Southern Hemisphere. The lower end is estimated with 39 parameters with a relatively large uncertainty. The emissions in summer are also lower by 20–30% than spring/fall. Considering the a posteriori uncertainties of >40%, it is not as statistically significant as the winter minimum.

[25] The a posteriori changes in the biomass-burning sources are subtler particularly in light of the a posteriori uncertainties. A general feature emerged from the 3 inversion cases is that the a priori NH biomass-burning source in the nonburning seasons (other than spring) is too high by 30%. As a result, the a posteriori biomass-burning source is lower and the NH to Southern Hemisphere (SH) emission ratio decreases from 1.7 to 1.1 (in the 11-parameter case).

[26] The a posteriori oceanic source increases by 60% to $\sim$800 Tg yr^{-1}. The a posteriori error is, however, as large as around 50%, which could be due to limited observations over the tropical/subtropical oceanic emission regions. The observational constraints on the other sources/sinks, which are relatively small in magnitude, are not very good. What is clear is the decreasing trend in the a posteriori results. The largest decrease is found in the 11-parameter case, the a posteriori sources/sinks are $\sim$1/3 of the a priori values.

[27] In the following sections, we examine the effects of a posteriori sources on the distributions of CH_3Cl. We first compare model simulations with surface measurements and then with aircraft measurements. The measurement sites and regions are shown in Figure 1.

3.1.2. Evaluation With Surface Measurements

[28] Seasonal variations of observed and simulated CH_3Cl at seven surface sites are shown in Figure 4. There is no significant difference among the inversion results with the three different parameter sizes. In the NH, the a priori model overestimates the observations at the middle and high latitudes through the year except in spring. In the a posteriori model, those positive biases are corrected mostly because of the decrease of the biogenic CH_3Cl emissions during winter. The a posteriori results, however, tend to underestimate at the NH sites in spring and early summer. These negative biases appear to be driven in part by the need to correct the a priori (positive) bias in the comparison to aircraft measurements. The a posteriori model improves significantly in the NH winter, reproducing better the observed seasonal minima. In the SH, the a posteriori model corrects the significant a priori positive bias at the three sites from June to November mainly because of the decrease of biogenic emissions during SH winter (June–August). However, the a posteriori model overestimates the seasonal variation at the SH sites.

[29] Figure 5 shows the annual and seasonal latitudinal distributions at these sites. The annual-mean latitudinal distribution is symmetric because the major sources of CH_3Cl are located in the tropics. These two features, symmetric distribution and major tropical sources, provide a useful constraint on the ratio of the NH to SH mean OH is within 20% of 1:1 [*Yoshida et al.*, 2004]. The seasonal mean CH_3Cl mixing ratios are high in the NH between December and May, reflecting lower OH concentrations in winter and the relatively long lifetime of >1 year. The a posteriori model corrects the a priori high biases in June–August in the SH, December–February in the NH, and most signifi-

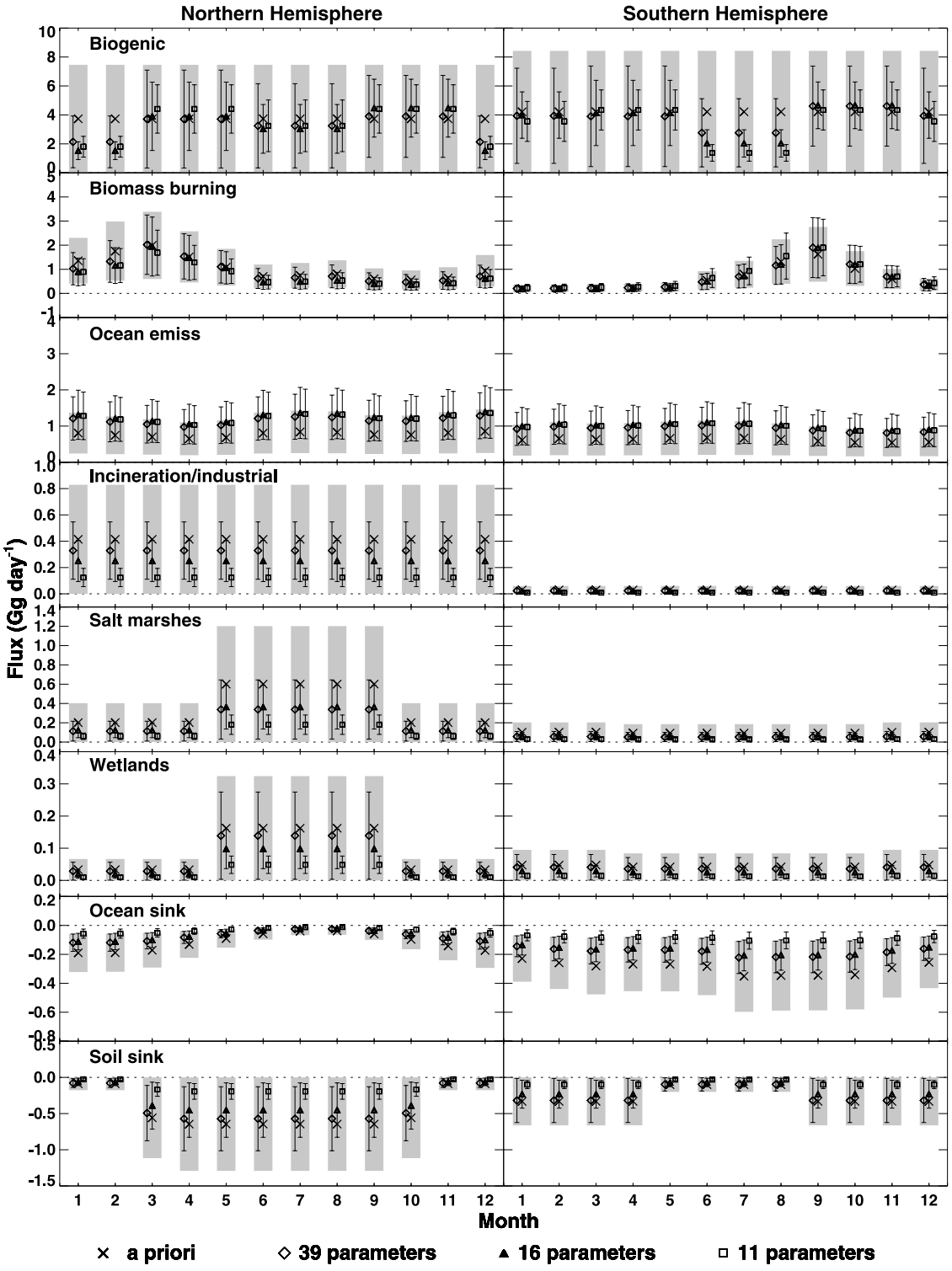

Figure 3. A priori and a posteriori monthly sources and sinks for the three cases with different model parameters (Table 3).

cantly in September–November in both hemispheres. However, the a posteriori model has a low bias in March–May over the tropics and the NH.

3.1.3. Evaluation With Aircraft Measurements

[30] As in the comparison with surface measurements, the a posteriori distributions over the aircraft measurement regions are very close in all three cases with different model parameter sizes. We therefore only show the results with 11 parameters in the state vector. Characteristics of CH_3Cl observed in the aircraft experiments have been discussed in detail by *Yoshida et al.* [2004]. We only compare the a priori with a posteriori model biases in the latitude-altitude cross

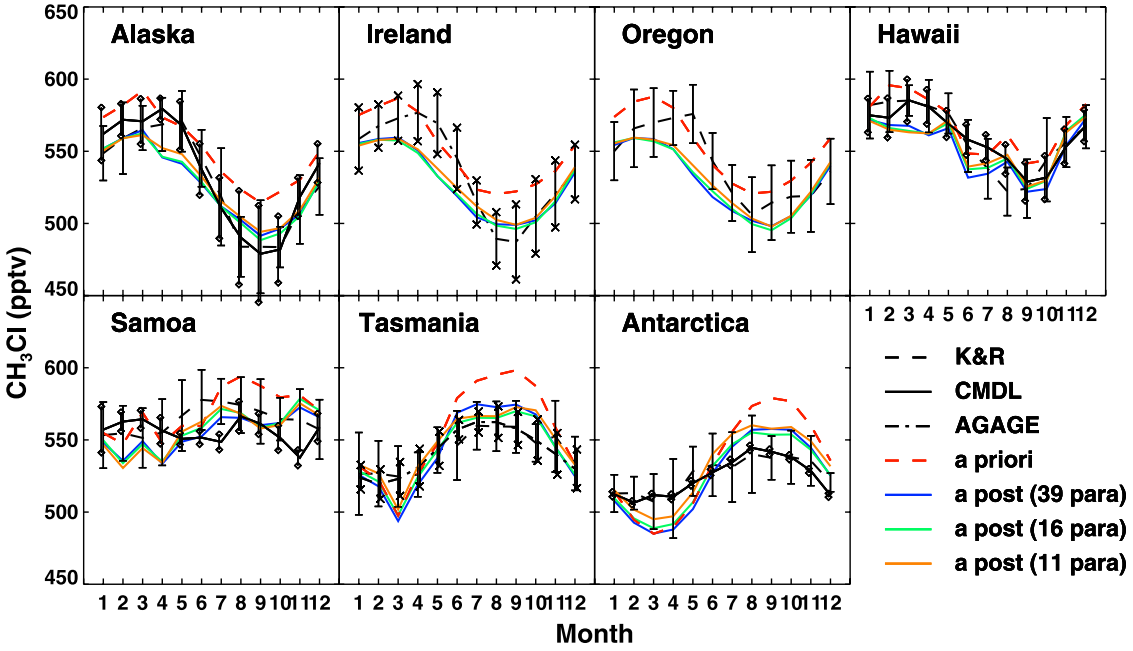

Figure 4. Seasonal variations of observed and simulated CH_3Cl at the surface sites. The vertical bars show the standard deviations of the measurements. Here, K&R, *Khalil and Rasmussen* [1999].

sections here (Figure 6). We discuss the comparison by region.

3.1.3.1. Tropical Pacific (Pacific Exploratory Mission–Tropics A and B)

[31] During Pacific Exploratory Mission (PEM)–Tropics A, our prior model overestimates the observations by 5 to 20% over the Fiji (fj), Tahiti (tht) and Hawaii (hwi) regions, especially in the northern sections (Figures 6a–6c). After the inversion, the biases are reduced to within ±5% over most of the observation points, reflecting the reductions of biogenic and biomass-burning CH_3Cl concentrations in our a posteriori model by 7–8% and 17–18% compared to the a priori values, respectively. For the eastern Pacific region (ep), the a priori model overestimates observations by > 20% because of biogenic and biomass-burning emissions and the positive bias remains after the inversion although the bias is reduced to <15% (Figure 6d).

[32] Figures 6e and 6f show the comparisons between the a priori and the a posteriori model biases for the PEM-Tropics B mission. For both Fiji and Tahiti regions, the a

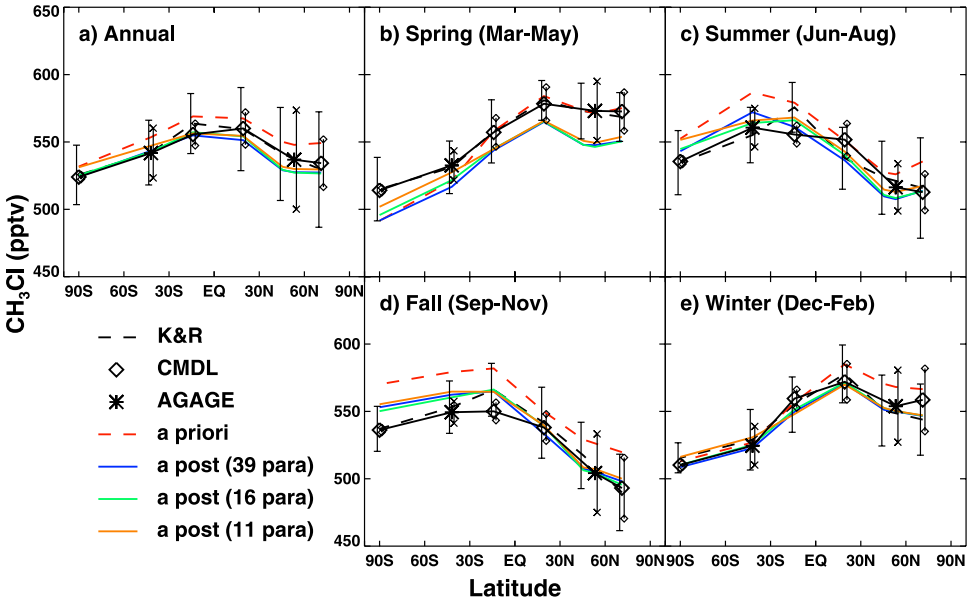

Figure 5. Latitudinal distributions of observed and simulated CH_3Cl at the surface sites. The vertical bars show the standard deviations of the measurements.

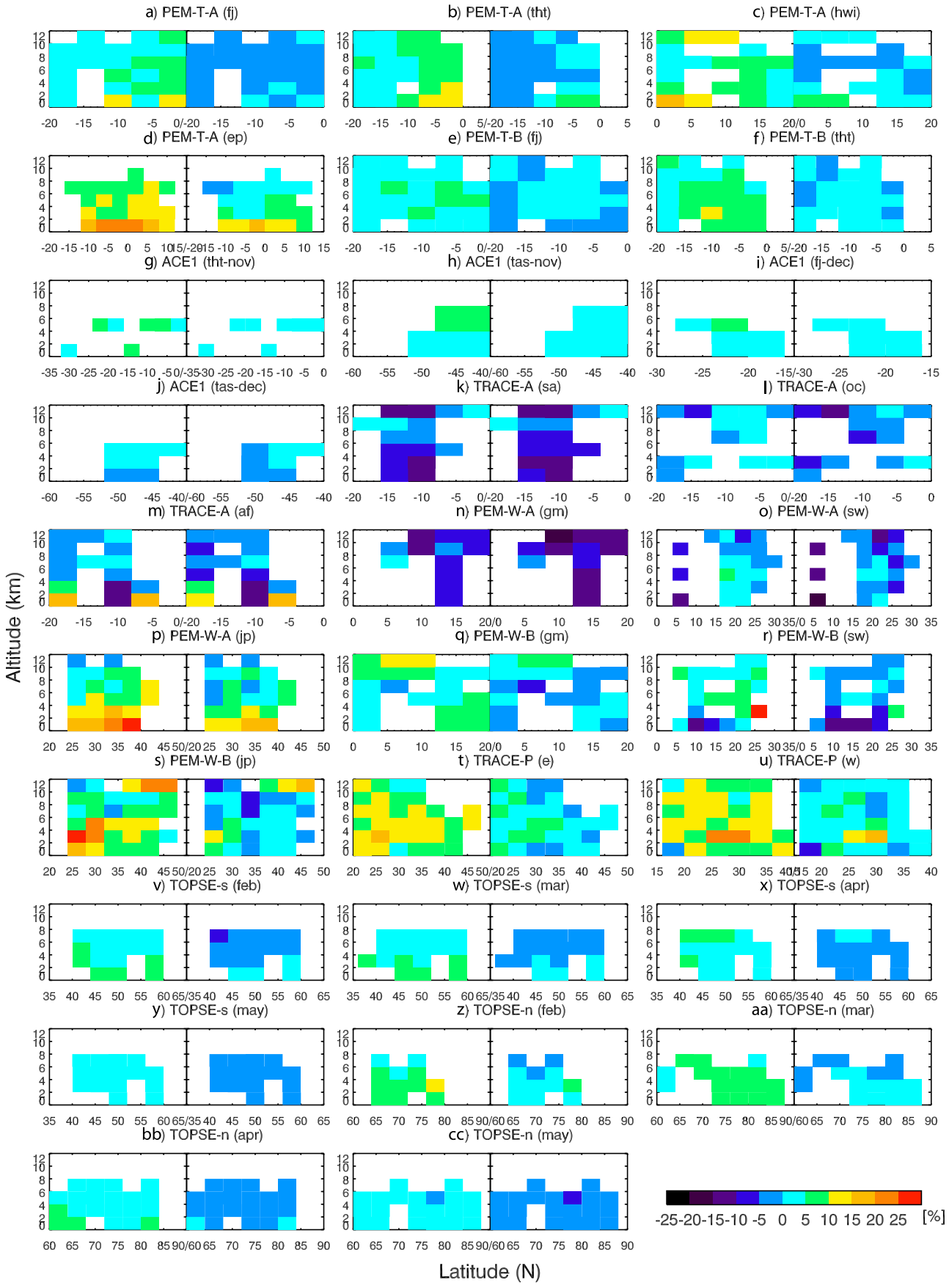

Figure 6. A priori and a posteriori relative biases computed as (model - observation)/observation with respect to aircraft observations as a function of latitude and altitude for regions shown in Figure 1.

posteriori model biases are reduced to within ±5%. Significant a priori overestimates near the surface in the Tahiti region between 4° and 12°S are reduced from 22% to 6% after the inversion, mainly reflecting the reduction of biogenic CH_3Cl concentrations.

3.1.3.2. Tropical Pacific and Southern Ocean (First Aerosol Characterization Experiment)

[33] During the First Aerosol Characterization Experiment (ACE 1), there are few observation points over the Tahiti-November (tht-nov) region (Figure 6g). Over the Tasmania-November (tas-nov) and Fiji-December (fj-dec) regions, the a priori model overestimates up to 8% especially at higher altitudes (Figures 6h and 6i). After the inversion, mean concentrations of biogenic CH_3Cl over these two regions are reduced by 50–70 pptv, resulting in a better agreement with the observations. For the Tasmania-December (tas-dec) region, both the a priori and the a posteriori models show small biases (Figure 6j).

3.1.3.3. Tropical Atlantic (Transport and Chemical Evolution Over the Atlantic)

[34] The Transport and Chemical Evolution over the Atlantic (TRACE-A) mission was designed to investigate the large effects of biomass-burning emissions observed over the South Atlantic, South America, and southern Africa. The a priori model result shows significant large (negative/positive) biases over the South America (sa) and southern Africa (af) regions (Figures 6k and 6m). In comparison, the a priori biases are generally within ±5% over the South Atlantic (oc) region (Figure 6l). *Yoshida et al.* [2004] suggested that the large underestimations by the model may be due in part to the biased samplings of biomass-burning plumes, which could not be reproduced in the simulated monthly mean concentrations. Consequently, the large biases are not corrected after the inversion. The coexistence of positive and negative biases in the TRACE-A regions also implies problematic spatial distributions of the biogenic and biomass-burning sources. However, as we discussed in the previous section (3.1.1), available measurements do not provide enough constraints on the continent-dependent CH_3Cl emissions.

3.1.3.4. Western Pacific (PEM-West A and B, Transport and Chemical Evolution Over the Pacific)

[35] Figures 6n–6p show the a priori and a posteriori model biases compared with PEM-West A observations. As discussed by *Yoshida et al.* [2004], during the PEM-West A, enhanced CH_3Cl concentrations were observed at high altitude (above 10 km) reflecting transport of CH_3Cl by typhoons, the effect of which could not be reproduced in our model. Our a priori model tends to underestimate the measurements at lower latitudes ($<\sim15°$) over the Guam (gm) and southwest (sw) regions. On the other hand, there are large positive biases (up to 26%) over the Japan (jp) region. The a posteriori mean concentrations are lower than the a priori values by ∼4% for the all three regions, which result in larger negative biases over the Guam and southwest regions and smaller positive biases over the Japan region. Those lower concentrations are due to a reduction of biogenic CH_3Cl by 10–15% than the prior, as well as a reduction of biomass-burning CH_3Cl by 10–16%.

[36] During PEM-West B, the a priori model overestimates observations by 5–27% in most regions except near the surface in the southwest (sw) region (Figures 6q–6s). Mean concentrations of the a posteriori results are less than the prior values by 5–7% because of smaller biogenic and biomass-burning CH_3Cl. Over the Guam (gm) region, the a posteriori biases are within ±7%. Over the southwest region, the a posteriori model shows improvements over much of the region except the underestimation at lower altitudes of up to 15%. The a posteriori biases over Japan region are reduced to within ±5% except in the lower troposphere at <30°N, where high concentrations are simulated in the model because of biogenic and biomass-burning CH_3Cl. High positive bases (<17%) above 10 km could be attributed to the relatively large uncertainties in the low-mixing-ratio measurements [*Yoshida et al.*, 2004].

[37] Figures 6t and 6u show the comparisons of a priori and a posteriori biases for the Transport and Chemical Evolution over the Pacific (TRACE-P) experiment over the eastern (e) and western (w) regions, respectively. There are significant a priori positive biases (>15%) over both regions below 4 km at 20°–35°N. The a posteriori biogenic and biomass-burning CH_3Cl mixing ratios are less than the a priori values by ∼60 and ∼20 pptv, respectively. Incineration/industrial CH_3Cl mixing ratios also decrease by ∼25 pptv over these regions. The positive biases are reduced in much of the regions except near 30°N in the western region.

3.1.3.5. North America (Tropospheric Ozone Production About the Spring Equinox)

[38] For the Tropospheric Ozone Production about the Spring Equinox (TOPSE) experiment, our a priori model biases are relatively small in comparison to other regions. After inversion, the positive biases of 5–10% in some regions are reduced to <5%. Overall, the posteriori results show very good agreement with the measurements.

3.2. Sensitivity to Surface and Aircraft Data Sets

[39] We examine here the constraints on CH_3Cl sources placed by surface in comparison to those by aircraft measurements. We apply inverse modeling to three different data sets: surface measurements only, aircraft measurements only, and the combination of surface and aircraft measurements. We use 11 model parameters in the state vector (Table 3) in these sensitivity tests.

[40] Figure 7 shows the a priori and a posteriori monthly fluxes in the three sensitivity cases. It is apparent that our best source estimates using both surface and aircraft measurements are closer to the results with aircraft measurements only than those with surface measurements only. The latter is closer to the a priori model, suggesting that the aircraft measurements offer better constraints on the CH_3Cl source estimates than surface measurements. For example, the a posteriori biogenic fluxes with surface measurements show almost no seasonal variations in the NH as the a priori model while the solution using aircraft measurements shows the winter minimum although both inversion results show the winter minimum in the SH. The a posterior oceanic source with surface measurements are similar to the a priori model while that with aircraft measurements indicates an increase of the source by 50–60%.

[41] We find 7, 9 and 10 significant singular values in the prewhitened Jacobian matrices with the measurements from surface, aircraft, and both surface and aircraft, respectively, providing additional evidence of better aircraft constraints.

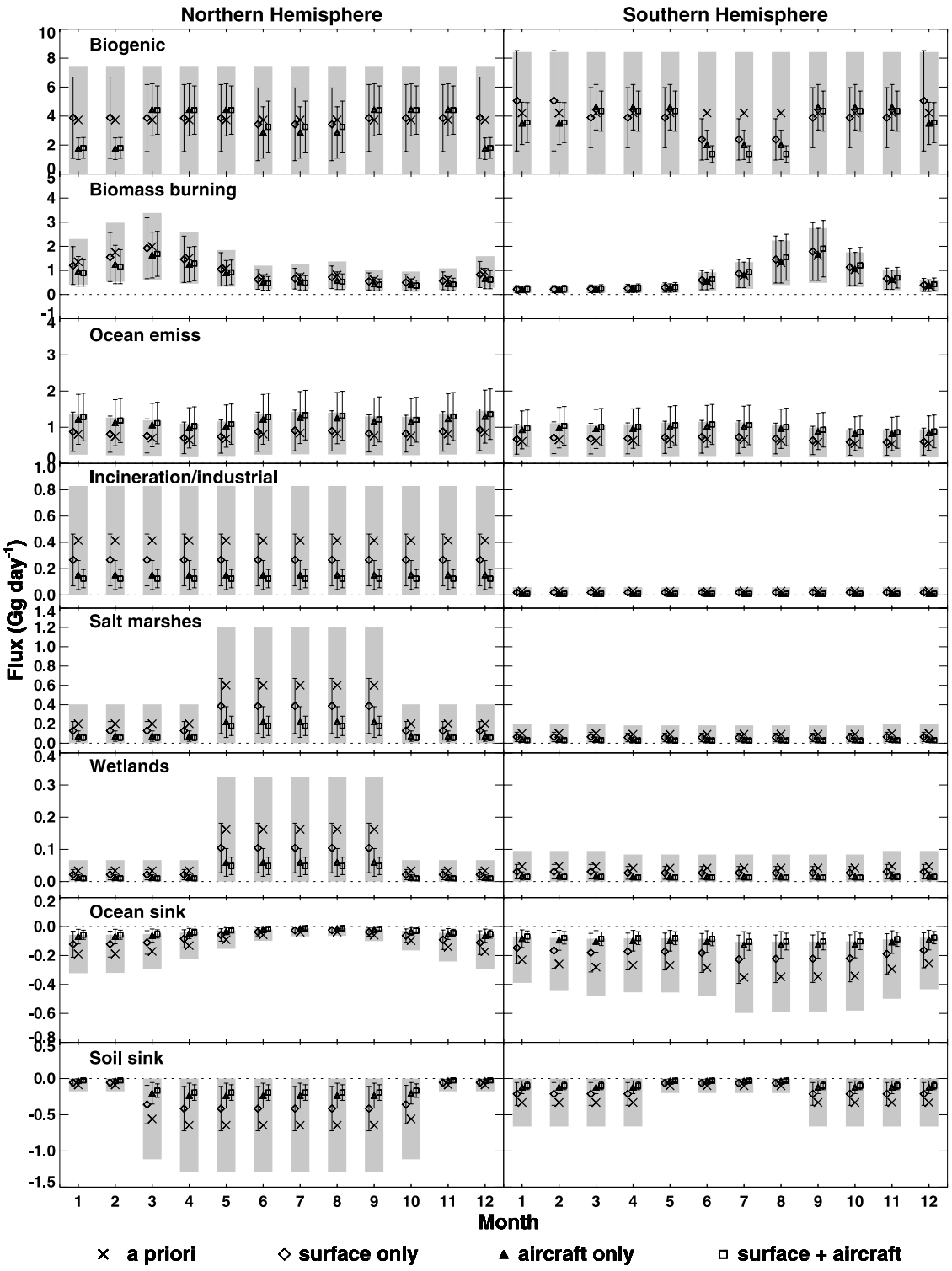

Figure 7. A priori and a posteriori monthly sources and sinks using the measurements from surface sites, aircraft, and both.

The closer proximity of aircraft measurements to the source regions appears to entail better constraints on the source estimates. The a priori model also shows larger discrepancies from the measurements. In comparison, the a prior model biases at the remote surface sites tend to be much smaller (particularly when considering the annual means), leading to relatively small changes in the a posteriori emissions.

4. Discussion

[42] We compare our a posteriori CH_3Cl sources with the a priori and literature values in this section. As detailed in

the previous section, our "best" inversion results are obtained using both surface and aircraft measurements with 11 model parameters. The a posteriori net flux is about 3850 Gg yr^{-1}, only ~4% less than the a priori value of 3990 Gg yr^{-1}, reflecting the relatively small change of the simulated global CH_3Cl concentrations.

[43] The annual total of the a posteriori biogenic CH_3Cl is about 2510±980 Gg yr^{-1} and about 13% less than the a priori estimate. Although the CH_3Cl emission estimates from tropical plants are still quite uncertain (820–8200 Gg yr^{-1}) [*Montzka et al.*, 2003], our results suggest that the biogenic source contributes to ~60% of the total global source.

[44] The a posteriori biomass-burning emission is 545 Gg yr^{-1}, which is about 11% less than the a priori estimate. It is much lower than the source of 910 (650–1120) Gg yr^{-1} estimated by *Lobert et al.* [1999]. The oceanic CH_3Cl source is estimated at 600 (325–1300) Gg yr^{-1} by *Khalil et al.* [1999]. Our a priori and a posteriori estimates are 507 and 806 Gg yr^{-1}, respectively. The other emissions and sinks including incineration/industrial, salt marshes and wetland sources, and ocean and soil sinks are smaller in the a posteriori estimates than the a priori by a factor of 3. However, available measurements do not provide enough information to invert these relatively small sources individually.

5. Conclusions

[45] We conduct Bayesian inversion analysis to constrain better CH_3Cl sources and sinks using the observations from seven surface sites and eight aircraft field experiments. The GEOS-Chem CTM is used as the forward model. We evaluate the sensitivities of the inversion results to the number of model parameters in the state vector and observation data set encompassing surface only, aircraft only, or both measurements.

[46] We first compile a "wish list" of 39 model parameters that among others resolve the continental and seasonal distributions of the biogenic source. However, the degree of freedom in the inversion is 10. We then construct a secondary inversion with 16 parameters by discarding for instance the continental dependence. By examining the structure of the singular vectors of the Jacobian matrix and considering the physical understanding of the source, we reduce the number of parameters to 11 by lumping correlated parameters together. The resulting degree of freedom in the inversion remains to be 10. The three inversion results show largely compatible results. As the number of model parameters gets close to the degree of freedom in the inversion, the a posteriori uncertainties tend to decrease. The best constraint on the biogenic emission estimates is obtained with 11 model parameters.

[47] Additional sensitivities are conducted to examine the constraints placed by surface and aircraft measurements. With only surface measurements, the a posteriori emissions are fairly close to the a priori. With only aircraft measurements, the a posteriori emissions are much closer to the results when both types of measurements are used, indicating that the a posteriori changes are driven mostly by aircraft measurements. The degree of freedom increases from 7 for surface measurements to 9 for aircraft measurements. To better constrain the temporal and spatial distributions of CH_3Cl emissions, aircraft and surface measurements near the major source regions are essential.

[48] The a posteriori model simulation shows significant improvement in comparison to surface and aircraft observations. The particularly large a priori positive bias at the SH surface sites in June–November is corrected with a posteriori emissions. Discrepancies between the a posteriori model and aircraft observations are generally within ±5% for most regions, except those locations strongly affected by local biogenic and biomass-burning CH_3Cl sources.

[49] The a posteriori biogenic source of 2.5 Tg yr^{-1} shows a clear winter minimum in both hemispheres; the a posteriori uncertainty is generally 30–40%. We find the variations among the other three seasons are smaller than a posteriori uncertainties. Our current knowledge on biogenic CH_3Cl production is insufficient to speculate on specific processes responsible to the winter minimum. The gross a posteriori oceanic emission is 810 Gg yr^{-1} with an uncertainty of ~50%, while the gross a posteriori oceanic sink is only 45 Gg yr-1 with an uncertainty of ~60%. Our best estimate of the biomass-burning source is ~550 Gg yr^{-1} with an uncertainty of ~60%. The most significant change in the a posteriori emissions is the large reduction of NH emissions of 82 Gg yr^{-1} in seasons other than spring. The a posteriori source decreases by 27% to 281 Gg yr^{-1} in the NH but increases by 17% to 264 Gg yr^{-1} in the SH. Our results could either indicate that the CH_3Cl/CO emission ratio is dependent on season and hemisphere or imply that the NH/SH ratio of biomass-burning CO emissions in the GEOS-Chem is overestimated due largely to an overestimate of the NH emissions in seasons other than spring.

[50] **Acknowledgments.** We thank Daniel Jacob and Colette Heald for their help. The GEOS-Chem model is managed at Harvard University with support from the NASA Atmospheric Chemistry Modeling and Analysis Program. This work was supported by the NASA ACMAP program.

References

Bey, I., D. J. Jacob, R. M. Yantosca, J. A. Logan, B. Field, A. M. Fiore, Q. Li, H. Liu, L. J. Mickley, and M. Schultz (2001), Global modeling of tropospheric chemistry with assimilated meteorology: Model description and evaluation, *J. Geophys. Res.*, *106*, 23,073–23,096.

Blake, N. J., D. R. Blake, B. C. Sive, T.-Y. Chen, F. S. Rowland, J. E. Collins Jr., G. W. Sachse, and B. E. Anderson (1996), Biomass burning emissions and vertical distribution of atmospheric methyl halides and other reduced carbon gases in the South Atlantic region, *J. Geophys. Res.*, *101*, 24,151–24,164.

Blake, N. J., D. R. Blake, T.-Y. Chen, J. E. Collins Jr., G. W. Sachse, B. E. Anderson, and F. S. Rowland (1997), Distribution and seasonality of selected hydrocarbons and halocarbons over the western Pacific basin during PEM-West A and PEM-West B, *J. Geophys. Res.*, *102*, 28,315–38,331.

Blake, N. J., et al. (1999a), Influence of southern hemispheric biomass burning on midtropospheric distributions of nonmethane hydrocarbons and selected halocarbons over the remote South Pacific, *J. Geophys. Res.*, *104*, 16,213–16,232.

Blake, N. J., et al. (1999b), Aircraft measurements of the latitudinal, vertical, and seasonal variations of NMHCs, methyl nitrate, methyl halides, and DMS during the First Aerosol Characterization Experiment (ACE 1), *J. Geophys. Res.*, *104*, 21,803–21,817.

Blake, N. J., et al. (2001), Large-scale latitudinal and vertical distributions of NMHCs and selected halocarbons in the troposphere over the Pacific Ocean during the March–April 1999 Pacific Exploratory Mission (PEM-Tropics B), *J. Geophys. Res.*, *106*, 32,627–32,644.

Blake, N. J., D. R. Blake, B. C. Sive, A. S. Katzenstein, S. Meinardi, O. W. Wingenter, E. L. Atlas, F. Flocke, B. A. Ridley, and F. S. Rowland (2003a), The seasonal evolution of NMHCs and light alkyl nitrates at middle to high northern latitudes during TOPSE, *J. Geophys. Res.*, *108*(D4), 8359, doi:10.1029/2001JD001467.

Blake, N. J., et al. (2003b), NMHCs and halocarbons in Asian continental outflow during the Transport and Chemical Evolution over the Pacific (TRACE-P) field campaign: Comparison with PEM-West B, *J. Geophys. Res.*, *108*(D20), 8806, doi:10.1029/2002JD003367.

Duncan, B. N., R. V. Martin, A. C. Staudt, R. Yevich, and J. A. Logan (2003), Interannual and seasonal variability of biomass burning emissions constrained by satellite observations, *J. Geophys. Res.*, *108*(D2), 4100, doi:10.1029/2002JD002378.

Hamilton, J. T. G., W. C. McRoberts, F. Keppler, R. M. Kalin, and D. B. Harper (2003), Chloride methylation by plant pectin: An efficient environmentally significant process, *Science*, *301*, 206–209.

Heald, C. L., D. J. Jacob, P. I. Palmer, M. J. Evans, G. W. Sachse, H. B. Singh, and D. R. Blake (2003), Biomass burning emission inventory with daily resolution: Application to aircraft observation of Asian outflow, *J. Geophys. Res.*, *108*(D21), 8811, doi:10.1029/2002JD003082.

Heald, C. L., D. J. Jacob, D. B. A. Jones, P. I. Palmer, J. A. Logan, D. G. Streets, G. W. Sachse, J. C. Gille, R. N. Hoffman, and T. Nehrkorn (2004), Comprehensive inverse analysis of satellite (MOPITT) and aircraft (TRACE-P) observations to estimate Asian sources of carbon monoxide, *J. Geophys. Res.*, *109*, D23306, doi:10.1029/2004JD005185.

Keene, W. C., et al. (1999), Composite global emissions of reactive chlorine from anthropogenic and natural sources: Reactive Chlorine Emissions Inventory, *J. Geophys. Res.*, *104*, 8429–8440.

Khalil, M. A. K., and R. A. Rasmussen (1999), Atmospheric methyl chloride, *Atmos. Environ.*, *33*, 1305–1321.

Khalil, M. A. K., R. M. Moore, D. B. Harper, J. M. Lobert, D. J. Erickson, V. Koropalov, W. T. Sturges, and W. C. Keene (1999), Natural emissions of chlorine-containing gases: Reactive Chlorine Emissions Inventory, *J. Geophys. Res.*, *104*, 8333–8346.

Koppmann, R., F. J. Johnen, D. Plass-Dülmer, and J. Rudolph (1993), Distribution of methyl chloride, dichloromethane, trichloroethene and tetrachloroethene over the North and South Atlantic, *J. Geophys. Res.*, *98*, 20,517–20,526.

Lee-Taylor, J. M., G. P. Brasseur, and Y. Yokouchi (2001), A preliminary three-dimensional global model study of atmospheric methyl chloride distributions, *J. Geophys. Res.*, *106*, 34,221–34,233.

Lobert, J. M., W. C. Keene, J. A. Logan, and R. Yevich (1999), Global chlorine emissions from biomass burning: Reactive Chlorine Emissions Inventory, *J. Geophys. Res.*, *104*, 8373–8389.

Martin, R. V., D. J. Jacob, R. M. Yantosca, M. Chin, and P. Ginoux (2003), Global and regional decreases in tropospheric oxidants from photochemical effects of aerosols, *J. Geophys. Res.*, *108*(D3), 4097, doi:10.1029/2002JD002622.

McCulloch, A., M. L. Aucott, C. M. Benkovitz, T. E. Graedel, G. Kleiman, P. M. Midgley, and Y. F. Li (1999), Global emissions of hydrogen chloride and chloromethane from coal combustion, incineration and industrial activities: Reactive Chlorine Emissions Inventory, *J. Geophys. Res.*, *104*, 8391–8403.

Montzka, S. A., et al. (2003), Controlled substances and other source gases, in *Scientific Assessment of Ozone Depletion: 2002*, *Global Ozone Res. Monit. Proj. Rep. 47*, chap. 1, p. I-1–I-83, World Meteorol. Organ., Geneva.

Moore, R. M., W. Groszko, and S. J. Niven (1996), Ocean-atmosphere exchange of methyl chloride: Results from NW Atlantic and Pacific Ocean studies, *J. Geophys. Res.*, *101*, 28,529–28,538.

Palmer, P. I., D. J. Jacob, D. B. A. Jones, C. L. Heald, R. M. Yantosca, J. A. Logan, G. W. Sachse, and D. G. Streets (2003), Inverting for emissions of carbon monoxide from Asia using aircraft observations over the western Pacific, *J. Geophys. Res.*, *108*(D21), 8828, doi:10.1029/2003JD003397.

Prinn, R. G., et al. (2001), Evidence for substantial variations of atmospheric hydroxyl radicals in the past two decades, *Science*, *292*, 1882–1888.

Rhew, R. C., B. R. Miller, and R. F. Weiss (2000), Natural methyl bromide and methyl chloride emissions from coastal salt marshes, *Nature*, *403*, 292–295.

Rhew, R. C., B. R. Miller, M. K. Vollmer, and R. F. Weiss (2001), Shrubland fluxes of methyl bromide and methyl chloride, *J. Geophys. Res.*, *106*, 20,875–20,882.

Rodgers, C. D. (2000), *Inverse Methods for Atmospheric Sounding*, World Sci., Hackensack, N. J.

Sander, S. P., A. R. Ravishankara, D. M. Golden, C. E. Kolb, M. J. Kurylo, M. J. Molina, G. K. Moortgat, and B. J. Finlayson-Pitts (2003), Chemical kinetics and photochemical data for use in stratospheric modeling: Evaluation 14, *JPL Publ.*, *02–25*.

Schneider, H. R., D. B. A. Jones, M. B. McElroy, and G.-Y. Shi (2000), Analysis of residual mean transport in the stratosphere: 1. Model description and comparison with satellite data, *J. Geophys. Res.*, *105*, 19,991–20,011.

Shorter, J. H., C. E. Kolb, P. M. Crill, R. A. Kerwin, R. W. Talbot, M. E. Hines, and R. C. Harriss (1995), Rapid degradation of atmospheric methyl bromide in soils, *Nature*, *377*, 717–719.

Simmonds, P. G., et al. (2004), AGAGE observations of methyl bromide and methyl chloride at Mace Head, Ireland, and Cape Grim, Tasmania, 1998–2001, *J. Atmos. Chem.*, *47*, 243–269.

Varner, R. K., P. M. Crill, and R. W. Talbot (1999), Wetlands: A potentially significant source of atmospheric methyl bromide and methyl chloride, *Geophys. Res. Lett.*, *26*, 2433–2436.

Watling, R., and D. B. Harper (1998), Chloromethane production by wood-rotting fungi and an estimate of the global flux to the atmosphere, *Mycol. Res.*, *102*, 769–787.

Yokouchi, Y., Y. Noijiri, L. A. Barrie, D. Toom-Sauntry, T. Machida, Y. Inuzuka, H. Akimoto, H.-J. Li, Y. Fujinuma, and S. Aoki (2000), A strong source of methyl chloride to the atmosphere from tropical coastal land, *Nature*, *403*, 295–298.

Yokouchi, Y., M. Ikeda, Y. Inuzuka, and T. Yukawa (2002), Strong emission of methyl chloride from tropical plants, *Nature*, *416*, 163–165.

Yoshida, Y., Y. Wang, T. Zeng, and R. Yantosca (2004), A three-dimensional global model study of atmospheric methyl chloride budget and distributions, *J. Geophys. Res.*, *109*, D24309, doi:10.1029/2004JD004951.

D. R. Blake, Department of Chemistry, University of California, 516 Rowland Hall, Irvine, CA 92697-2025, USA.

D. Cunnold, C. Shim, Y. Wang, and Y. Yoshida, School of Earth and Atmospheric Sciences, Georgia Institute of Technology, 311 Ferst Drive, Atlanta, GA 30332-0340, USA. (yyoshida@eas.gatech.edu)

G. S. Dutton, NOAA/CMDL, Mail Stop R E CG1, 325 Broadway, Boulder, CO 80303, USA.